NASA Technical Memorandum 107273

Effects of Fiber Content on Mechanical Properties of CVD SiC Fiber-Reinforced Strontium Aluminosilicate Glass-Ceramic Composites

Narottam P. Bansal
Lewis Research Center
Cleveland, Ohio

July 1996

National Aeronautics and
Space Administration

Effects of Fiber Content on Mechanical Properties of CVD SiC Fiber-Reinforced Strontium Aluminosilicate Glass-Ceramic Composites

Narottam P. Bansal
National Aeronautics and Space Administration
Lewis Research Center
Cleveland, OH 44135

Abstract

Unidirectional CVD SiC_f(SCS-6) fiber-reinforced strontium aluminosilicate (SAS) glass-ceramic matrix composites containing various volume fractions, ~16 to 40 volume %, of fibers were fabricated by hot pressing at 1400°C for 2 h under 27.6 MPa. Monoclinic celsian, $SrAl_2Si_2O_8$, was the only crystalline phase formed, with complete absence of the undesired hexacelsian phase, in the matrix. Room temperature mechanical properties were measured in 3-point flexure. The matrix microcracking stress and the ultimate strength increased with increase in fiber volume fraction, reached maximum values for $V_f \sim 0.35$, and degraded at higher fiber loadings. This degradation in mechanical properties is related to the change in failure mode, from tensile at lower V_f to interlaminar shear at higher fiber contents. The extent of fiber loading did not have noticeable effect on either fiber-matrix debonding stress, or frictional sliding stress at the interface. The applicability of micromechanical models in predicting the mechanical properties of the composites was also examined. The currently available theoretical models do not appear to be useful in predicting the values of the first matrix cracking stress, and the ultimate strength of the SCS-6/SAS composites.

1. INTRODUCTION

Advanced materials having high specific strength, high fracture toughness, and resistance to oxidizing and other adverse environments are needed for various high temperature structural applications in the aerospace and other industries. Continuous ceramic fiber-reinforced ceramic matrix composites are being developed to address these stringent requirements. Efforts are underway in different research laboratories around the world for the development of various

ceramic, glass, and glass-ceramic matrices reinforced with advanced ceramic fibers for high temperature structural applications. Glass ceramics having monoclinic celsian as the crystalline phase appear to be the most refractory glass ceramic with a projected use temperature of ~1600°C. Celsian is oxidation resistant, has good thermal shock resistance because of its low thermal expansion coefficient of ~2.5 x 10^{-6}/°C, and does not undergo any phase transformation up to ~1590°C. Therefore, at NASA Lewis, celsian glass-ceramics are being investigated as a prospective matrix material for fiber-reinforced composites for applications as high temperature structural materials in hot sections of turbine engines.

Processing details and various properties of the CVD SiC monofilament reinforced celsian glass-ceramic matrix composites have been described by the present author[1-3]. The objective of the present study was to investigate the effects of fiber volume content on the mechanical properties of unidirectional CVD SiC_f (SCS-6) fiber-reinforced $SrAl_2Si_2O_8$ (SAS) glass-ceramic matrix composites. Various mechanical properties such as matrix microcracking stress, elastic modulus, ultimate strength, fiber/matrix interfacial shear stress, and frictional sliding stress have been measured. The experimentally measured values of first matrix cracking stress and ultimate strength as a function of fiber content have also been compared with those predicted from the currently available theoretical models.

2. MATERIALS AND EXPERIMENTAL METHODS

2.1. Materials

Strontium aluminosilicate glass of stoichiometric celsian composition, $SrO.Al_2O_3.2SiO_2$ (SAS), was used as precursor to the matrix. The glass was melted at ~2000°C in a continuous electric melter with Mo electrodes using laboratory grade $SrCO_3$, Al_2O_3, and SiO_2. Homogeneous and clear glass flakes were produced by quenching the melt between water-cooled metallic rollers. Attrition milling of the glass frit using alumina media in the presence of Darvan as a surfactant resulted in glass powder having an average particle size of ~2.5 μm . From wet chemical analysis, the composition of the glass powder was determined in weight percent to be 33.7 SrO, 31.5 Al_2O_3, 33.8 SiO_2, 0.12 Na_2O, and 0.86 BaO. The Mo was estimated at 0.01 wt % MoO_3 by a spectrographic technique. The batch composition in weight percent was 31.8 SrO, 31.3 Al_2O_3, and 36.9 SiO_2, which corresponds to stoichiometric celsian.

Continuous SiC SCS-6 monofilaments from Textron Specialty Materials having a diameter of ~142 μm were used as the reinforcements. The schematic of the cross-section and the surface region of the fiber are shown in Fig. 1. These fibers are produced by chemical vapor deposition (CVD) of SiC onto a pyrolytic graphite-coated carbon core having a diameter of 37 μm. The fiber is made up of two distinct zones. The inner zone consists[4] of carbon-rich β-SiC columnar grains extending in the radial direction with < 111 > preferred orientation and lengths of a few micrometers. The outer zone consists of nearly stoichiometric β-SiC grains. The average grain diameter changes from ~50 nm in the inner zone to ~100 nm in the outer zone[4]. The surface of the fibers is coated with a dual carbon-rich SiC layer (Fig. 1). At room temperature, these fibers typically have an elastic modulus of ~400 GPa and tensile strength of ~3.9 GPa. The average axial thermal expansion coefficient of these fibers, from room temperature to 1000°C, is ~4.4 x 10^{-6}/°C.

2.2. Composite Fabrication

Unidirectional fiber-reinforced composite (FRC) panels ~112.5 mm x 50 mm x 1.25 mm (4½" x 2" x 0.05") containing various volume fractions of the fibers were fabricated using a glass-ceramic approach to take advantage of the viscous flow of the glass during hot pressing. Details of this method are described elsewhere[1-3,5]. An aqueous slurry of SAS glass powder along with organic additives was cast into tapes using a Doctor blade and allowed to dry in ambient atmosphere. The dry tape, ~0.15 mm thick, was cut to size. The fiber mats were cut to size from tape prepared by winding continuous SiC fibers on a drum with a spacing of 41 fibers per cm. Adhesive tape was used to hold the fibers in place. Matrix tapes and fiber mats were alternately stacked up in the desired orientation and warm pressed. The resulting "green" composite was wrapped in Mo sheet and then in grafoil and hot pressed under vacuum in a graphite die at 1400°C for 2 h under a pressure of 27.6 MPa. The fugitive binder was burned out before hot pressing by holding at a lower temperature. Pressure was first applied at 900°C during hot pressing The resulting FRC panels were surface polished and sliced into flexure test bars using a high speed diamond blade saw.

2.3. Characterization

Densities were measured by the Archimedes method as well as from specimen dimensions and weight. The fiber volume fraction, V_f, in the composite was determined from

$$V_f = N_f \pi r_f^2 / Wd \quad (1)$$

where N_f is the number of fibers, r_f is the fiber radius assumed to be 71 μm, W and d are respectively the width and thickness of the specimen. The crystalline phases formed in the glass-ceramic matrix were identified from powder x-ray diffraction (XRD) patterns recorded at room temperature using a step scan procedure (0.03°/2θ step, count time 0.5 s) on a Phillips ADP-3600 automated powder diffractometer equipped with a crystal monochromator and employing copper K_α radiation. Mechanical properties of the composites were determined from stress-strain curves recorded in three-point flexure, rather than four-point bending, because tensile fracture rather than interlaminar shear failure is the more likely failure mode in three-point bend tests. An Instron machine at a crosshead speed of 0.127 cm/min (0.05 in./min) was used. In one case, the effect of test span length (L) to sample thickness (d) ratio on first matrix cracking stress and ultimate strength of the composite was also investigated. A value of L/d >25 was used in subsequent strength measurements with span length of the lower rollers of 3.75 cm (1.5 in.). The first matrix cracking stress and the elastic modulus of the composites were determined from strain gauges glued to the tensile surface of the test bars. A discontinuous jump in strain in the load vs. strain plot indicated matrix cracking. Matrix cracking was also indicated by a kink in the load vs. time output of the chart recorder. Values of first matrix cracking stress obtained from the two techniques were in good agreement. Elastic modulus was determined from the linear portion of the load vs. strain curve up to the first matrix cracking load. Microstructures of the polished cross-sections as well as fracture surfaces were observed in an optical microscope and/or in a JEOL JSM-840A scanning electron microscope (SEM).

Fiber/matrix interfacial shear strength (ISS) and frictional sliding stress were determined from a fiber push-out test using thin polished sections of the composites cut normal to the fiber axis. The indenter, a 100 μm diameter flat-bottomed tungsten carbide punch, was aligned over a single fiber and was driven at a constant speed of 50 μm/min. The specimen was supported so

that the fiber being pushed out can protrude out of the bottom of the sample without any obstruction. A load cell constantly monitors the load as the punch is pushed mechanically. Load data were collected at 50 ms intervals by a computer. Conversion of time to actual crosshead displacement allows a load versus displacement curve to be generated as the output of the push-out test. About twenty fibers were pushed out in different regions of the FRC. The push-out apparatus had an upper load limit of 40 N.

3. RESULTS AND DISCUSSION

3.1 Microstructure

SEM micrographs taken from polished cross-sections of the composites containing various volume fractions of the reinforcing fibers are shown in Fig. 2. Overall uniform fiber distribution and good matrix flow around the fibers during hot pressing is observed in all composites. At high fiber loadings, fiber-fiber contact can be observed. X-ray diffraction analysis showed the presence of β-SiC fibers and the desired monoclinic $SrAl_2Si_2O_8$ celsian phase matrix in the composites.

3.2. Mechanical Properties

Typical stress vs. displacement curves for a hot pressed SAS monolithic and unidirectional CVD SiC_f/SAS composite are shown in Fig. 3. The monolithic SAS, hot pressed at 1200°C for 2 h at 24 MPa, shows a flexural strength of ~130 MPa and fails in a brittle mode as expected. The stress-displacement curve for the SCS-6/SAS composite, hot pressed at 1400°C for 2 h at 24 MPa, shows graceful failure. It consists of an initial linear elastic region followed by matrix microcracking with a first matrix cracking stress, σ_y, of ~289 MPa. Beyond this, there is an extended nonlinear regime of increasing load bearing capacity as most of the reinforcing fibers are still intact and undamaged, and carry additional load. The ultimate strength, σ_u, is ~824 MPa. At higher loads, fiber fracture and pull out occurs, and the load bearing capacity of the composite decreases as fewer and fewer fibers are left intact to carry the load. These results clearly demonstrate that reinforcement of the SAS glass-ceramic with SCS-6 fibers results in tough and strong composites.

When the ratio of the test span length to sample thickness ratio is high enough to minimize

the shear forces during testing, the value of matrix fracture stress obtained from the flexure test is equivalent to that measured in tension because matrix cracking is the first damage to occur[6] in the composite. The effect of test span length (L) to sample thickness (d) ratio on the first matrix cracking stress and the ultimate strength measured in three-point flexure are shown in Fig. 4 for the SCS-6/SAS composite. Both σ_y and σ_u increase sharply with initial increase in L/d ratio, but strength levels off at L/d $> \sim 25$. At high L/d ratio, the sample failure occurred on the tensile surface where the tensile stresses are the highest, whereas delamination was observed at low L/d. All further flexure measurements were carried out using an L/d ratio of greater than 25.

Effect of fiber content on first matrix cracking stress, elastic modulus, and ultimate strength, measured in 3-point flexure, of SCS-6/SAS composites hot pressed at 1400°C for 2 h under 27.6 MPa pressure are listed in Table I. Figure 5 compares measured values of the elastic modulus with those calculated from the rule of mixtures using the relationship

$$E_c = V_m E_m + V_f E_f \qquad (2)$$

where E is the elastic modulus, V is the volume fraction and the subscripts c, m, and f refer to the composite, matrix, and fiber, respectively. Values of 70 GPa and 400 GPa were used in the calculations for the elastic modulii of the SAS glass-ceramic matrix and the SCS-6 fibers, respectively. The solid line represents the results obtained from equation (2). The measured E_c values are in agreement with those expected from the simple rule of mixtures. For SCS-6 fiber-reinforced zircon matrix composites also, the values of composite elastic modulus measured in three-point flexure and tensile tests are reported[7] to be similar and followed the rule of mixtures.

Variations in first matrix cracking stress and ultimate strength of the composites with the fiber content are shown in Figure 6. Values of both σ_y and σ_u increased with the fiber content, reached a maximum at $V_f \sim 0.35$ and dropped with further increase in V_f.

The current theoretical models[8-11] predict an increase in strength of the continuous fiber-reinforced ceramic matrix composites with increase in fiber content. The composite strength is

also expected to improve with increase in fiber strength and frictional sliding stress of the fiber/matrix interface. The presence of higher volume per cent of reinforcing fibers results in greater overall load bearing capacity and an increase in the fiber/matrix interface along which fiber sliding can occur. A drop in strength of the composites at higher fiber loadings is unexpected from the theory[8-11]. The degradation in matrix microcracking stress and ultimate strength at high fiber contents, observed in the present study, can be explained by the change in failure mode of the composite, from tensile at low V_f to interlaminar shear at high V_f. The composites having $V_f \sim 0.4$ were observed to fail in shear (Fig. 7) whereas those having lower fiber content failed in tension. It appears that in the presence of a higher volume fraction of the fibers, the interlaminar shear strength of the composite is degraded resulting in lower values of first matrix cracking stress and ultimate strength.

A similar change in failure mode has also been observed by Singh *et al.*[12] who investigated the influence of fiber content on flexural properties of SiC (SCS-6) fiber-reinforced reaction-bonded silicon nitride (RBSN) composites. The matrix microcracking stress, ultimate strength, and work of fracture increased with fiber content, reached a maximum for ~ 16 volume per cent of fiber and decreased with higher loading of the fibers. No fiber damage was observed during composite processing due to lower temperatures used during composite fabrication. The degradation in properties at higher fiber content was explained by a change in failure mode to interlaminar shear rather than fiber pullout observed at lower fiber volume fraction. The 16 volume per cent of fibers is probably too low a fiber loading for the mechanical properties to peak out.

In SiC (SCS-6)/RBSN composites, Bhatt *et al.*[13,14] reported an increase in first matrix cracking stress and strain measured in tension at room temperature for fiber contents of 8 to 34 volume per cent. However, value of the ultimate tensile strength reached a maximum for $V_f \sim$ 24 - 30 % and degraded for composites having higher fiber content. This was ascribed to poor matrix infiltration between the fibers resulting in large voids in the matrix. However, recently Xu *et al.*[15] found that for a hot pressed Si_3N_4 matrix reinforced with CVD SiC (SCS-6) fibers, the composite strength increased with fiber volume fraction from 0.14 to 0.29. When the fiber content was raised to 55%, the composite strength dropped due to degradation in fiber strength

as a result of damage to fibers from contact with surrounding fibers and abrasive matrix particles during hot pressing. For a hot pressed Si_3N_4 matrix reinforced with CVD SiC (SCS-2) monofilaments, Shetty *et al.*[16] found that the composite strength was virtually independent of the fiber volume fraction from $V_f \sim 0.05$ to 0.45. For hot pressed ceramic grade Nicalon reinforced pyrex glass composites, Dawson *et al.*[17] found that composite strength increased linearly with fiber volume fraction from 0.2 to 0.6. Hegeler and Bruckner[18] reported that for Nicalon/glass composites made by hot pressing, the composite strength increased with fiber content, reaching a maximum at $V_f = 0.5$ and then dropped rapidly for higher V_f. However, for the SCS-6/SAS glass-ceramic matrix composites of the present study, values of first matrix cracking stress and ultimate strength increased with the fiber loading, reaching a maximum for $V_f \sim 0.35$ and dropping for higher V_f, due to a change in failure mode from tensile to interlaminar shear.

3.3. Fiber/Matrix Interface

SEM micrographs showing magnified views of the fiber/matrix interface in the unidirectional SCS-6/SAS composites are presented in Fig. 8. The interface is clean and the carbon rich double coating on the SCS-6 fiber surface is unaffected. This indicates no chemical interaction between the fiber and the matrix during high temperature composite processing.

In order to achieve high strength and, in particular, high toughness in the fiber-reinforced ceramic matrix composites, the fiber/matrix interfacial shear strength must be tailored such that the bond is strong enough to allow transfer of load from the matrix to the fibers, but weak enough so that an advancing matrix microcrack can be deflected at the interface by fiber/matrix debonding. To evaluate the fiber-matrix interfacial shear strengths (ISS), fiber push out tests were carried out. Typical fiber push out load vs. crosshead displacement curves for SCS-6/SAS glass-ceramic matrix composites with $V_f = 0.16$ and 0.35 are presented in Fig. 9. Similar curves were obtained for composites having 0.20 and 0.40 fiber volume fractions. The initial linear region corresponds to the elastic response of the material. The peak load, P_{debond}, corresponds to the fiber/matrix debonding load and the sudden drop in load represents debonding of the fiber. A sharp peak in the acoustic emission signal is also observed corresponding to the fiber/matrix debonding event. Following debonding, the slight increase in load corresponds to additional debonding. At the maximum load, the entire length of the fiber has debonded and the

fiber begins to exit from the opposite face of the composite. The steady state load represents the sliding friction at the interface. The load at 10 s after the acoustic emission peak was taken as the frictional load and used to calculate the frictional sliding stress. The slow and continuous decrease in load is due to the decrease in embedded length of the fiber.

Values of the fiber-matrix ISS for debond (τ_{debond}) and frictional sliding stress ($\tau_{friction}$) were calculated from

$$\tau = P/(2\pi r_f L_f) \quad (3)$$

where τ is the fiber-matrix interfacial shear strength, r_f is the radius of the fiber, L_f is the length of the embedded fiber, and P is the load corresponding to debond or friction. This equation assumes a uniform interfacial shear stress along the length of the fiber/matrix interface. A plot of fiber/matrix debonding load vs. sample thickness for the SCS-6/SAS composite is given in Fig. 10. The fiber debonding load varies linearly with the thickness of the sample used for fiber push out tests as expected from eq. (3). Effect of sample thickness on fiber-matrix debonding stress and frictional sliding stress is presented in Table II. Values of τ_{debond} and $\tau_{friction}$ evaluated from fiber push out tests for composites having various fiber volume % are listed in Table III. Values shown are the mean values for 20 push out tests. The value of τ_{debond} decreases and $\tau_{friction}$ increases (Table III) as the fiber loading is increased.

The presence of residual stresses in the composite can have significant influence on the fiber/matrix interfacial shear strength. These residual stresses can arise from various sources, but mainly come from thermal expansion mismatch between the fiber and the matrix as discussed later in this paper. When $\alpha_f > \alpha_m$, as in the composite system of the present study, the fiber-matrix interfacial region is under tension in the composite upon cooling from the processing temperature. If there is poor bonding at the interface, this may result in fiber separation from the matrix, as suggested by the similar values for τ_{debond} and $\tau_{friction}$ for the composites in the present study. In any case, a low interfacial shear strength typically results in a fibrous failure mode and a tough composite which, indeed, is the case for the composite of the present study. Similar values of τ_{debond} and $\tau_{friction}$ indicate that the fiber/matrix interface in SCS-6/SAS composites is frictionally coupled, i.e., the interfacial bonding is negligible.

SEM micrographs showing in-place and pushed out fibers in SCS-6/SAS composites are shown in Fig. 11. The surface of the pushed out fibers appears to be smooth. The carbon-rich double coating on the SCS-6 fiber is still intact. Debonding occurs between the matrix and the outer carbon rich coating applied on the SCS-6 fiber surface. Also, there appears to be no chemical interaction or interdiffusion between the SCS-6 fiber and the matrix during high temperature composite processing. Particles on fiber surfaces and the matrix are believed to be debris from sample preparation.

3.4. Comparison with Micromechanical Models

It is interesting to compare the measured values of the first matrix cracking stress and ultimate strength with those predicted from the theoretical models currently available. By using a simple energy balance approach, similar to that of Griffith in determining the stress necessary to propagate cracks in brittle solids, the following equation[8,9] has been derived for the first matrix cracking stress in a composite consisting of a low failure strain matrix reinforced with high failure strain continuous fibers:

$$\sigma_y = [(12\tau_{friction}\,\Gamma_m\,V_f^2\,E_f\,E_c^2)/\{r_f V_m E_m^2\}]^{1/3} \quad (4)$$

where Γ_m is the matrix fracture surface energy and other terms have the same meaning as above. It is apparent from this equation that the first matrix cracking stress can be enhanced by increasing fiber-matrix interfacial sliding stress, by using fibers of smaller radius, and by increasing the volume fraction of fibers. It might also be increased, less easily, by increasing E_f or by decreasing E_m. The matrix microcracking may also be suppressed by placing the matrix in compression through choosing $\alpha_f > \alpha_m$, although for isotropic fibers this will result in radial contraction of the fibers away from the matrix and a potential decrease in fiber-matrix shear strength. It is important to optimize the fiber-matrix bond strength carefully as too strong a bond will result in a brittle composite with low toughness. Typical values of Γ_m for ceramics range from 20 to 40 J/m^2 as quoted by Briggs and Davidge[19]. Values of Γ_m for calcium aluminosilicate and lithium aluminosilicate glass-ceramic matrices have been reported to be 25 and 20-30 J/m^2, respectively. Taking $\Gamma_m \approx 25$ J/m^2 for the SAS glass ceramic matrix, $E_f = 400$ GPa, $E_m = 70$ GPa, $r_f = 71$ μm, and appropriate values of other parameters as shown above, σ_y for the SCS-

6/SAS composites having various volume fractions of fibers were calculated from eq. (4). These values are listed in Table IV. The calculated values of σ_y are lower than those measured in three-point flexure except for the composite containing 40 volume % of fibers. However, it may be pointed out that generally the tensile strengths are lower than those measured in bending and the tensile test results, rather than the flexural data, are more meaningful for comparison with the predictions of the micromechanical models. Also, the effects of internal residual stresses arising from the thermal expansion mismatch between the fiber and the matrix, which have been neglected in the calculations of the ACK model[8], must be taken into account.

The axial residual stress in the matrix, σ_m, as a result of cooling from the composite hot pressing temperature is given by[20]

$$\sigma_m = [E_f V_f (\alpha_f - \alpha_m) \Delta T]/[1 + V_f(E_f/E_m - 1)] = [E_f V_f (\alpha_m - \alpha_f) \Delta T] [E_m/E_c] \quad (5)$$

where α_m and α_f are the thermal expansion coefficients of the matrix and the fibers, respectively, ΔT is the temperature range over which the composite has been cooled after processing, and the other terms are the same as described above. For composites of the present study, hot pressed at 1400°C, where $\alpha_f > \alpha_m$, the values of axial residual stress, σ_m, in the matrix at room temperature calculated from eq. (5) will be negative. The negative σ_m implies that the SAS glass-ceramic matrix will be in compression as fibers try to shrink more than the matrix and the residual stresses will be beneficial by tending to close the incipient matrix cracks.

As mentioned earlier, the residual stresses present in the as-manufactured composite are not considered in the derivation of eq. (4). Thermal residual stress present in the composite, $\Delta\sigma_c$, is given by the expression

$$\Delta\sigma_c = \sigma_m . (E_c/E_m) = E_f V_f (\alpha_m - \alpha_f) \Delta T \quad (6)$$

Calculated values of $\Delta\sigma_c$ at room temperature, using values of various parameters as $\alpha_f = 4.4 \times 10^{-6}/°C$, $\alpha_m = 2.5 \times 10^{-6}/°C$, are presented in Table IV. Negative residual thermal stresses indicate the compressive nature of the residual stresses in the composite of the present study. To

account for the residual stress effects in the composite due to fiber-matrix thermal expansion mismatch, the compressive stresses calculated from eq. (6) should be added to those determined from eq. (4). These modified values of σ_y corrected for the residual stresses are also given in Table IV. These corrected values of σ_y are much higher than those measured experimentally in three-point flexure. Also, the tensile test results, rather than the flexural data, are more meaningful for comparison with the predictions from the micromechanical models and generally the tensile strengths are lower than the flexural strengths. This would result in greater discrepancy between the calculated and the measured tensile strength data. Hence, the ACK model[8] does not appear to be useful in predicting the first matrix cracking stress for the large diameter fiber-reinforced SAS glass-ceramic composites of the present study. However, similar values of τ_{debond} and $\tau_{friction}$ (Table III) probably indicate that, due to a large thermal expansion mismatch between the fibers and the matrix, the fibers in the composite have already debonded from the matrix. This may result in elimination of thermal residual stresses in the SCS-6/SAS composites when cooled to room temperature after hot pressing.

An analytical estimate of the ultimate tensile strength of a fiber-reinforced composite is given by the equation[10,11]:

$$\sigma_u = V_f \sigma_f [\{1/(m+2)\}^{1/(m+1)} \{(m+1)/(m+2)\}] [2\tau_{friction} L_o/(\ln 2)\sigma_f r_f]^{1/m+1} \quad (7)$$

where V_f is volume fraction of fibers in the loading direction, r_f is the fiber radius, σ_f is the mean fiber tensile strength at a gauge length of L_o, m is the Weibull modulus, and $\tau_{friction}$ is the frictional sliding stress at the fiber-matrix interface. Equation (7) takes into account the proper gauge length of fibers relevant to composite tensile failure as well as the fiber bundle failure in brittle matrix composites. In eq. (7), the first two terms, $V_f \sigma_f$, give the rule-of-mixtures strength of the composite using the mean fiber strength at the test gauge length L_o. The third term within brackets is the statistical bundle-like factor depending only on m. This factor describes the tendency of the statistically weaker fibers to control the composite failure and the counteracting fact that broken fibers still have substantial load-carrying capability due to the sliding resistance $\tau_{friction}$. Thus, the first three terms together essentially give the bundle rule-of-mixtures strength of the FRC. The last term, called the composite factor, in eq. (7) accounts for the change in

fiber strength from gauge length L_o to the characteristic gauge length relevant to composite tensile failure and for the load carried by the broken fibers in brittle matrix composites. The composite factor is critical for predicting an accurate value of σ_u for the composite. Tensile strengths of SCS-6 fibers have been recently measured by various researchers[21-23]. Taking values of σ_f = 4170 MPa, m = 5.2, L_o = 4 cm, r_f = 71 μm for the SCS-6 fibers from a recent study[22], values of σ_u for the SCS-6/SAS composites containing various volume fractions of fibers were calculated from eq. (7). These values are listed in Table IV. The calculated values of σ_u are in reasonable agreement with those measured in 3-point flexure, except for the composite containing 40 volume % of fibers. However, the ultimate strengths of composites measured in flexure are reported[7,24,25] to be always higher than those measured in tension, by a factor of between 1.5 and 2.5 depending on lay-up. This is generally ascribed to the differences in stress distributions in the test specimens during flexure and tensile tests. During tensile testing, the entire gauge section is under tensile loading, but only a part of the sample is under tension during flexure test. The Curtin micromechanical model[10,11] is based on the assumption of uniaxial tensile loading. Thus, this would result in the measured ultimate strength values much lower than those predicted from the Curtin model.

Another reason for the discrepancy between the measured and predicted values of σ_u could be the fiber strength degradation occurring during composite fabrication. The strength of fibers after high temperature composite processing should be used in eq. (7). However, the strength of the *in situ* fibers in the FRC following hot pressing is unknown unless fibers can be extracted from the composite without further damage and tensile tested. The etchants used to dissolve away the celsian matrix from the SiC_f/SAS composite would invariably damage the fiber surface. Also, the abrasive damage to the fiber surface and other interactions occurring during high temperature composite processing may reduce fiber strength. For example, the strength of Nicalon fibers is 3 GPa, but the strength of the fibers extracted from Nicalon/Pyrex composites following processing at ~950°C is reduced by ~50%[25]. The degradation in the fiber strength depends on the temperature and pressure used during processing as well as on the reactivity between the fiber and the matrix. The room temperature strength of the SCS-6 fibers remained unchanged at ~5.5 GPa after 1 h exposure in 0.1 MPa argon pressure at 1400°C, but its strength did degrade[26] after heat treatments at higher temperatures.

4. SUMMARY

Effects of fiber content on room temperature mechanical properties of CVD SiC (SCS-6) fiber-reinforced strontium aluminosilicate glass-ceramic matrix composites have been investigated. Unidirectional composites containing 16 to 40 volume % of fibers were fabricated by hot pressing at 1400°C for 2 h at 27.6 MPa. Values of the first matrix cracking stress, elastic modulus, and ultimate strength measured in three-point flexure increased with increase in fiber content, reached maximum values for ~35 volume % fibers, and degraded at higher fiber loadings. This degradation in mechanical properties is related to the change in failure mode, from tensile at lower fiber loading to interlaminar shear at higher fiber contents. The fiber-matrix interfacial shear stress or the frictional sliding stress did not show any noticeable change with fiber volume fraction. The usefulness of theoretical models in predicting values of the first matrix cracking stress and the ultimate strength of the composites has also been evaluated.

5. CONCLUSIONS AND FUTURE WORK

Reinforcement of ceramic matrices with continuous fibers results in improvement of mechanical properties only up to a certain optimum fiber loading. Higher fiber contents lead to degradation of the composite mechanical properties. The micromechanical models currently available do not appear to be useful in predicting values of the first matrix cracking stress and the ultimate strength of the large diameter fiber-reinforced strontium aluminosilicate glass-ceramic composites tested in flexure.

Future research will involve the processing and mechanical, microstructural, and fiber/matrix interface characterization of SAS glass-ceramic matrix composites with advanced small diameter multifilament tow fibers such as the Hi-Nicalon, Hi-Nicalon type S, or the Dow Corning stoichiometric SiC fibers as reinforcement.

Acknowledgments

Thanks are due to John Setlock, Sharon Thomas, and Myles McQuater for their technical assistance during composite processing and/or characterization.

References

1. Bansal, N. P., "Method of Producing a Silicon Carbide Fiber Reinforced Strontium Aluminosilicate Glass-Ceramic Matrix Composite," U. S. Patent 5,389,321, February 14, 1995.

2. Bansal, N. P., "Ceramic Fiber Reinforced Glass-Ceramic Matrix Composite," U. S. Patent 5,214,004, May 25, 1993.

3. Bansal, N. P., "Processing and Properties of CVD SiC Fiber-Reinforced $BaAl_2Si_2O_8$ Glass-Ceramic Matrix Composites," in Proc. of 17th Conference on Metal Matrix, Carbon, and Ceramic Matrix Composites, Cocoa Beach, FL, Jan. 10-15, 1993; NASA CP 3235, Part 2, pp. 773 - 797 (1994).

4. Wawner, F.W., Teng, A.Y., and Nutt, S.R., "Microstructural Characterization of SiC (SCS) Filaments," *SAMPE Quart.*, **14**[3] 39-45 (1983).

5. Bansal, N.P., "Strontium Aluminosilicate Glass-Ceramic Composites Reinforced With Uncoated CVD SiC Fibers," NASA TM 106672 (1994).

6. Marshall, D.B., and Evans, A.G., "Failure Mechanisms in Ceramic-Fiber/Ceramic Matrix Composites," in *"Ceramic Containing Systems"*, A.G.Evans, Ed., Noyes Publications, Park Ridge, NJ, 1986, pp. 90-123.

7. Singh, R.N., "Influence of Testing Method on Mechanical Properties of Ceramic Matrix Composites," *J. Mater. Sci.*, **26**[23] 6341-6351(1991).

8. Aveston, J., Cooper, G. A., and Kelly, A., "Single and Multiple Fracture," in The Properties of Fiber Composites, Proceedings of the Conference, Teddington, Middlesex, England; IPC Technology and Science Press, 1971; pp. 15 -26.

9. Budiansky, B., Hutchinson, J.W., and Evans, A.G., "Matrix Fracture in Fiber-Reinforced Ceramics," *J. Mech. Phys. Solids*, **34**[2] 167-189 (1986).

10. Curtin, W.A., "Theory of Mechanical Properties of Ceramic-Matrix Composites," *J. Am. Ceram. Soc.*, **74**[11] 2837-45 (1991).

11. Curtin, W.A., "Ultimate Strengths of Fiber-Reinforced Ceramics and Metals," *Composites*, **24**[2] 98-102 (1993).

12. Singh, D., Singh, J. P., and Bhatt, R. T., "Influence of Fiber Content on Mechanical Performance of SiC-Fiber-Reinforced Reaction-Bonded Silicon Nitride Composites," *Ceram. Eng. Sci. Proc.*, **16**[4] 445-458 (1995).

13. Baaklini, G. Y. and Bhatt, R. T., "In-Situ X-Ray Monitoring of Damage Accumulation in SiC/RBSN Tensile Specimens," NASA TM 103733 (1991).

14. Bhatt, R. T., "Tension, Compression, and Bend Properties for SiC/RBSN Composites," in Composites: Design, Manufacture, and Application," (S. W. Tsai and G. S. Springer, Eds.), Proc. 8th Int. Confr. Comp. Mater., SAMPE, 1991, pp. 23A1 - 23A13.

15. Xu, H. H. K., Ostertag, C. P., Braun, L. M., and Lloyd, I. K., "Effect of Fiber Volume Fraction on Mechanical Properties of SiC-Fiber/Si_3N_4-Matrix Composites," *J. Am. Ceram. Soc.*, **77**[7], 1897-900 (1994).

16. Shetty, D. K., Pascucci, M. R., Mutsuddy, B. C., and Wills, R. R., "SiC Monofilament-Reinforced Si_3N_4 Matrix Composites," *Ceram. Eng. Sci. Proc.*, **6**[7-8], 632-45 (1985).

17. Dawson, D. M., Preston, R. F., and Purser, A., "Fabrication and Materials Evaluation of High Performance Aligned Ceramic Fiber-Reinforced Glass Matrix Composite," *Ceram. Eng. Sci. Proc.*, **8**[7-8], 815-21 (1987).

18. Hegeler, H. and Bruckner, R., "Fiber-Reinforced Glasses: Influence of Thermal Expansion of the Glass Matrix on Strength and Fracture Toughness of the Composites," *J. Mater. Sci.*, **25**[11], 4836-46 (1990).

19. Briggs, A. and Davidge, R.W., "Borosilicate Glass Reinforced with Continuous Silicon Carbide Fibers: A New Engineering Ceramics," *Mater. Sci. Eng.*, **A109**, 363-372 (1989).

20. Phillips, D.C., Sambell, R.A.J., and Bowen, D.H., "The Mechanical Properties of Carbon Fiber Reinforced Pyrex Glass," *J. Mater. Sci.*, **7**, 1454-1464 (1972).

21. Draper, S.L., Brindley, P.K., and Nathal, M.V., "Effect of Fiber Strength on the Room Temperature Tensile Properties of SiC/Ti-24Al-11Nb," *Metall. Trans. A*, **23A**, 2541-48 (1992).

22. Martineau, P., Lahaye, M., Pailler, R., Naslain, R., Couzi, M., and Cruege, F., "SiC Filament/Titanium Matrix Composites Regarded as Model Composites. Part 1. Filament Microanalysis and strength Characterization," *J. Mater. Sci.*, **19**[8] 2731-48 (1984).

23. MacKay, R.A., Draper, S.L., Ritter, A.M., and Siemers, P.A., "A Comparison of the Mechanical Properties and microstructures of Intermetallic Composites Fabricated by Two Different Methods," *Metall. Trans. A*, **25A**[7] 1443-1455 (1994).

24. Bleay, S.M., Scott, V.D., Harris, B., Cooke, R.G. and Habib, F.A., "Interface Characterization and Fracture of Calcium Aluminosilicate Glass-Ceramic Reinforced with Nicalon Fibers," *J. Mater. Sci.*, **27**[10] 2811-2822 (1992).

25. Prewo, K.M., "Tension and Flexural Strength of Silicon Carbide Fiber Reinforced Glass Ceramics," *J. Mater. Sci.*, **21**[10], 3590-3600 (1986).

26. Bhatt, R.T., and Hull, D.R., "Microstructural and Strength Stability of CVD SiC Fibers in Argon Environment," NASA TM 103772, 1991.

Table I. Influence of Fiber Content on Mechanical Properties of CVD SiC_f(SCS-6)/SAS Composites Measured in 3-Point Flexure [Hot Pressed 1400°C, 2 h, 27.6 MPa]

Composite #	V_f, %	σ_y, MPa	E_c, GPa	σ_u, MPa
---	0.0	---	70	130
SAS 10-6-93	16	163±3	124±7	477±26
SAS 9-7-93	20	211±35	139±8	531±27
SAS 8-6-93	35	332±43	216±14	861±33
SAS 9-13-93[a]	40	225±24	200±17	524±79

Average values for 4-5 test bars.
[a] Samples with V_f = 40% failed in shear. Other samples failed in tension.

Table II. Effect of Sample Thickness on Fiber-Matrix Interface Shear Strength and Sliding Frictional Stress Evaluated from Fiber Push-out for CVD SiC_f(SCS-6)/SAS Composites Hot Pressed at 1400° C for 2 h Under 27.6 MPa; V_f = 0.31 #SAS 6-1-93

Sample thickness, mm	Interface shear strength[a], τ_{debond}, MPa	Sliding frictional stress[a], $\tau_{friction}$, MPa
1.31	6.7 (2.3)	3.7 (1.0)
1.74	6.6 (0.7)	4.4 (0.6)
1.84	7.0 (0.7)	4.2 (0.3)
2.57	6.6 (0.5)	4.3 (0.3)

[a]Mean value for 8-10 fibers. Values in parenthesis are standard deviation.

Table III. Effect of Fiber Content on Fiber-Matrix Interface Shear Strength and Sliding Frictional Stress Evaluated from Fiber Pushout for CVD SiC_f(SCS-6)/SAS Composites [Hot Pressed 1400°C, 2h, 27.6 MPa]

Composite #	Sample thickness mm	V_f %	Interface shear strength[a] τ_{debond}, MPa	Sliding Frictional stress[a] $\tau_{frictional}$, MPa
SAS 10-6-93	1.87	16	7.5 (0.6)	4.8 (0.3)
SAS 9-7-93	1.87	20	6.4 (0.5)	3.9 (0.2)
SAS 6-1-93	1.31 - 2.57	31	6.7 (0.5)	4.2 (0.3)
SAS 8-6-93	1.87	35	6.2 (0.5)	4.4 (0.3)
SAS 9-13-93	1.87	40	5.6 (0.6)	4.5 (0.4)

[a]Mean values for 20 fibers; values in parenthesis are standard deviations

Table IV. Measured and Calculated Values of Room Temperature Mechanical Properties of CVD SiC_f(SCS-6)/SAS Composites Hot Pressed at 1400°C for 2 h at 27.6 MPa

V_f, %	Residual stresses[a] MPa	σ_y, MPa			σ_u, MPa	
		Measured[b]	ACK model eq.(4)	ACK model + residual stress[a]	Measured[b]	Curtin's model eq. (7)
16	-168	163 ± 3	91	259	477 ± 26	462
20	-210	211 ± 35	107	317	531 ± 27	559
35	-367	332 ± 43	214	581	861 ± 33	997
40	-420	225 ± 24	256	676	524 ± 79	1144

[a]Residual thermal stresses calculated from eq. (6).
[b]Measured in three-point flexure.

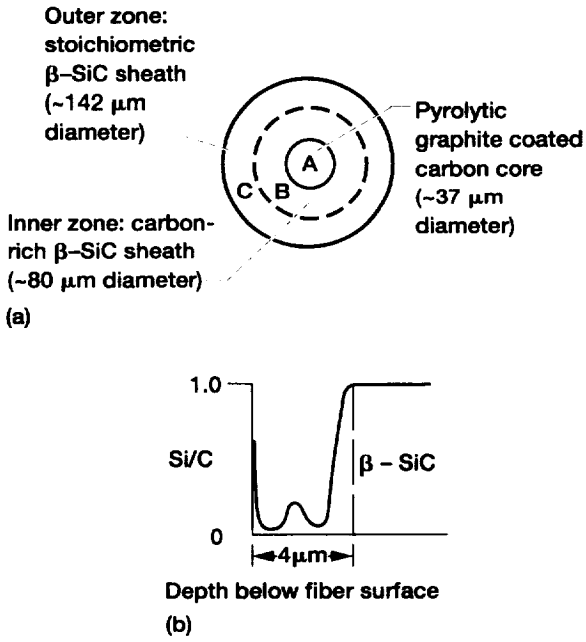

Figure 1.—Schematics showing cross-section and surface region of Textron CVD SiC SCS-6 monofilament. (a) Cross-section. (b) Surface region.

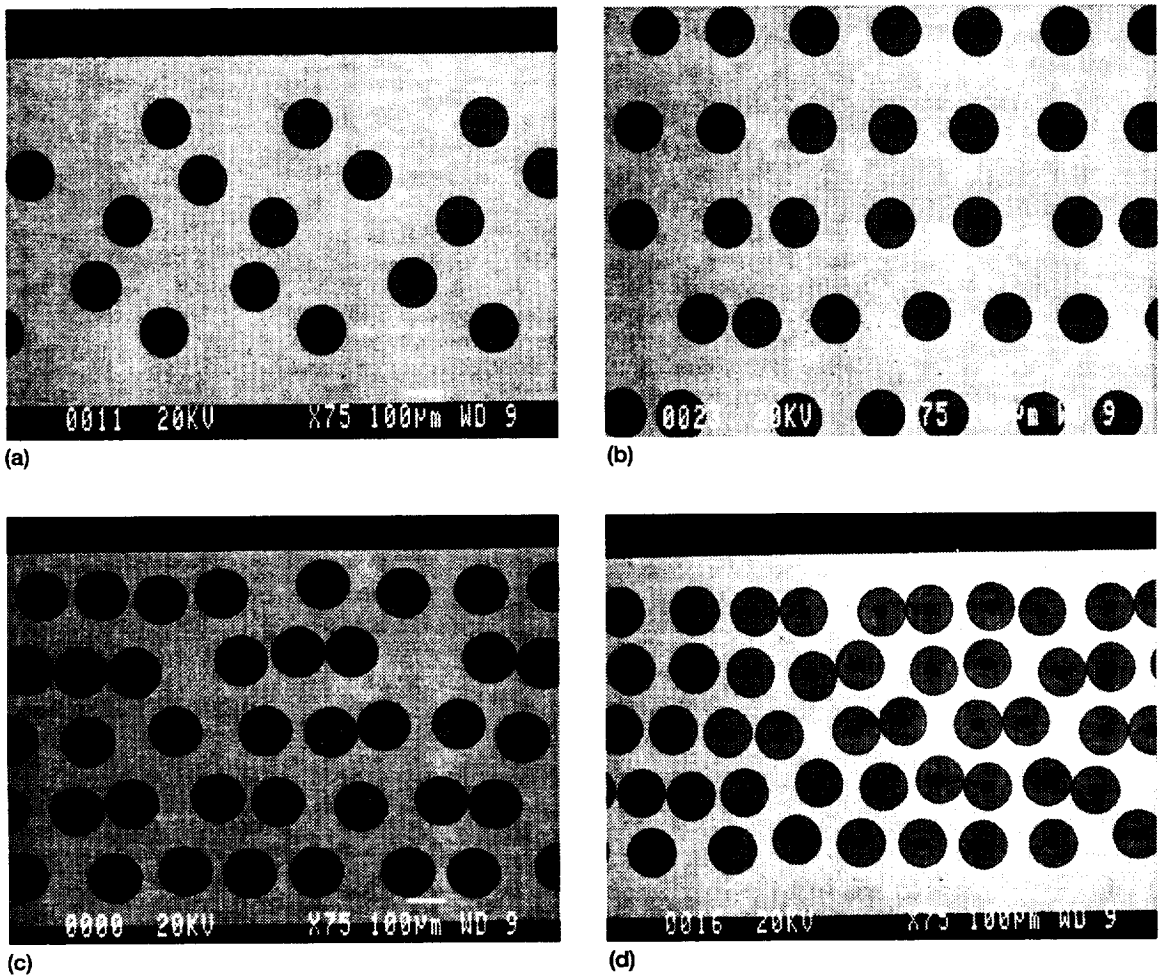

Figure 2.—SEM micrographs showing polished cross-sections of unidirectional CVD SiC (SCS-6) fiber-reinforced SAS glass-ceramic composites having various fiber contents; hot pressed at 1400 °C for 2 hr under 27.6 MPa. (a) V_f = 16 percent. (b) V_f = 20 percent. (c) V_f = 35 percent. (d) V_f = 40 percent.

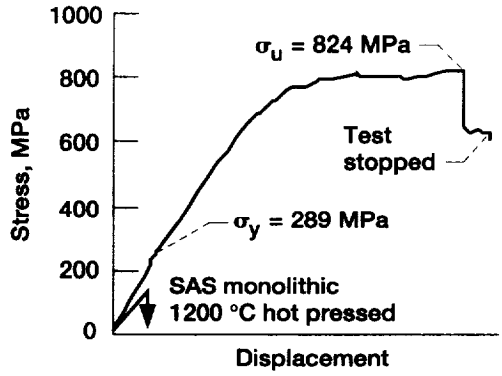

Figure 3.—Stress-displacement curves of SAS monolithic hot pressed at 1200 °C for 2 hr under 24 MPa and a unidirectional CVD SiC_f (SCS-6)/SAS composite hot pressed at 1400 °C for 2 hr under 24 MPa. The monolithic glass-ceramic was tested in four point bend, and the composite in three point flexure, respectively.

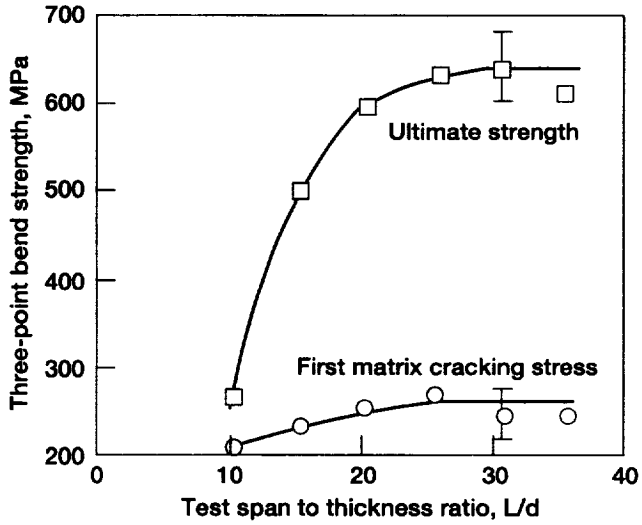

Figure 4.—Effect of test span length to sample thickness ratio (L/d) on first matrix cracking stress and ultimate strength, measured in three point flexure, for a unidirectional CVD SiC_f (SCS-6)/SAS composite hot pressed at 1350 °C for 2 hr at 24 MPa; V_f = 0.25. One test/data point except for L/d = 32 where five specimens were tested.

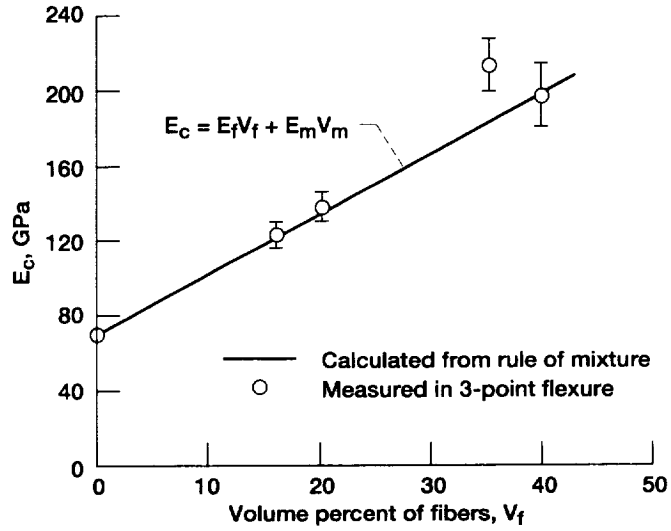

Figure 5.—The comparison of elastic modulus measured in three point bend with those calculated from the rule of mixtures for unidirectional CVD SiC_f (SCS-6)/SAS composites with various fiber volume contents hot pressed at 1400 °C for 2 hr at 27.6 MPa

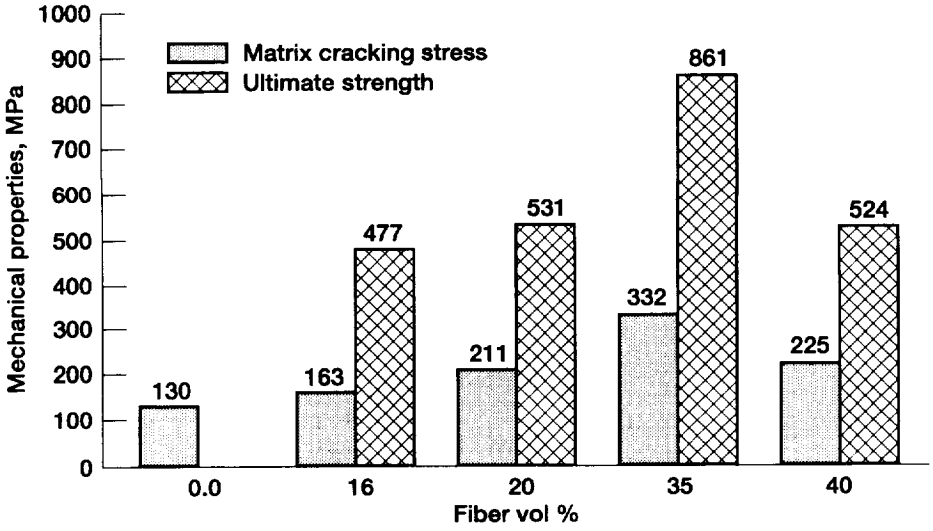

Average values for 4-5 test bars.
Samples with V_f = 40% failed in shear; others failed in tension

Figure 6.—Effect of fiber content on matrix microcracking stress and ultimate strength, measured in three point flexure at room temperature, for unidirectional CVD SiC_f (SCS-6)/SAS composites hot pressed at 1400 °C for 2hr at 27.6 MPa.

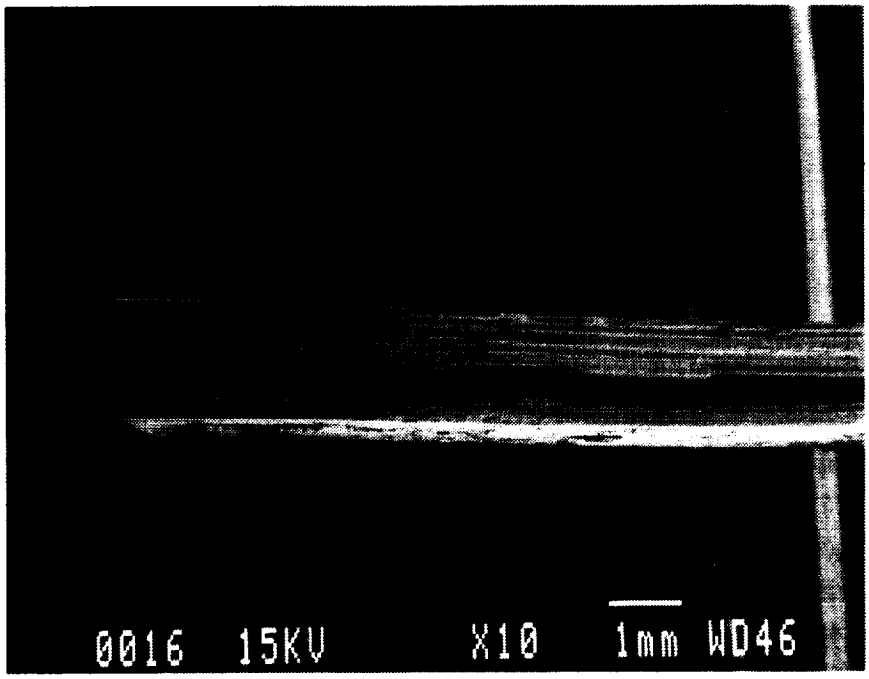

Figure 7.—SEM micrograph showing interlaminar shear failure in unidirectional CVD SiC (SCS-6)/SAS composite after three point bend test; $V_f = 0.4$.

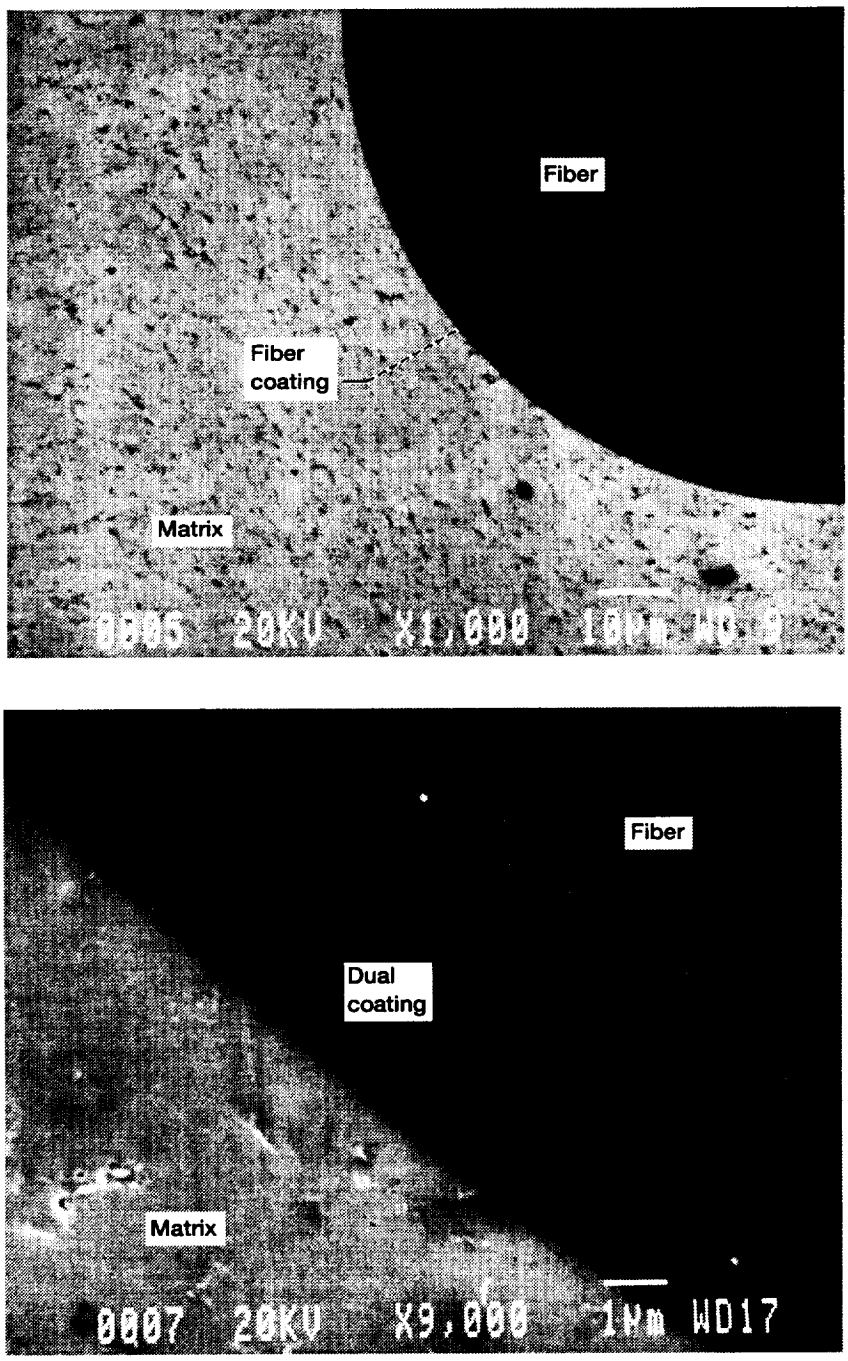

Figure 8.—SEM micrographs showing magnified views of the fiber-matrix interface in CVD SiC_f (SCS-6)/SAS composite hot pressed at 1400 °C for 2 hr at 27.6 MPa; $V_f = 0.35$.

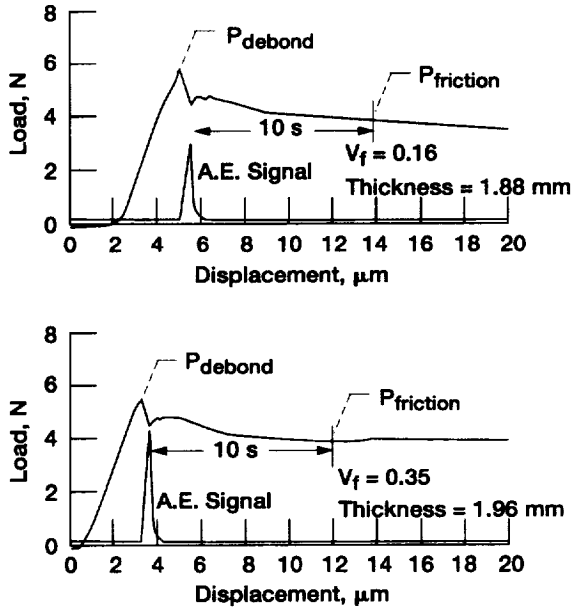

Figure 9.—Typical load vs. crosshead displacement curves recorded during fiber pushout in CVD SiC_f (SCS-6)/SAS composites with V_f = 0.16 and 0.35, hot pressed at 1400 °C for 2 hr at 27.6 MPa.

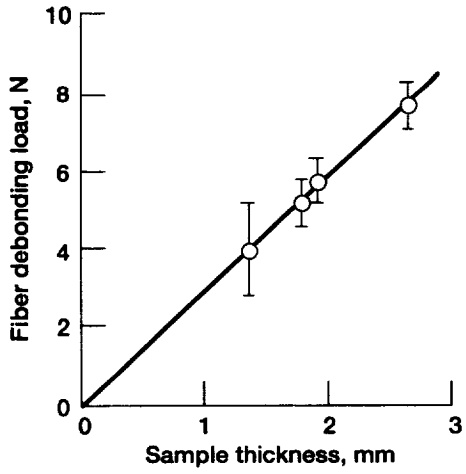

Figure 10.—Effect of sample thickness on fiber/matrix debonding load for CVD SiC_f (SCS-6)/SAS composite hot pressed at 1400 °C for 2 hr at 27.6 MPa.

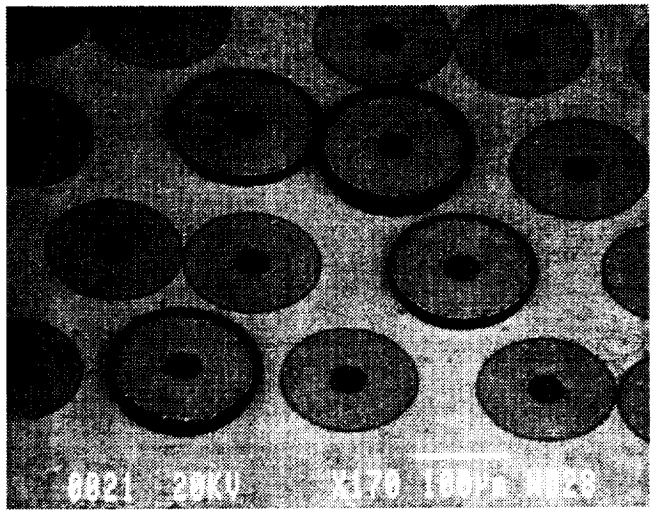

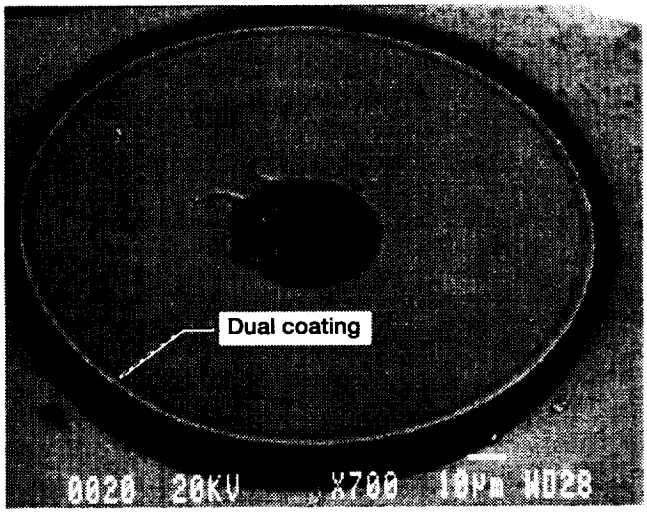

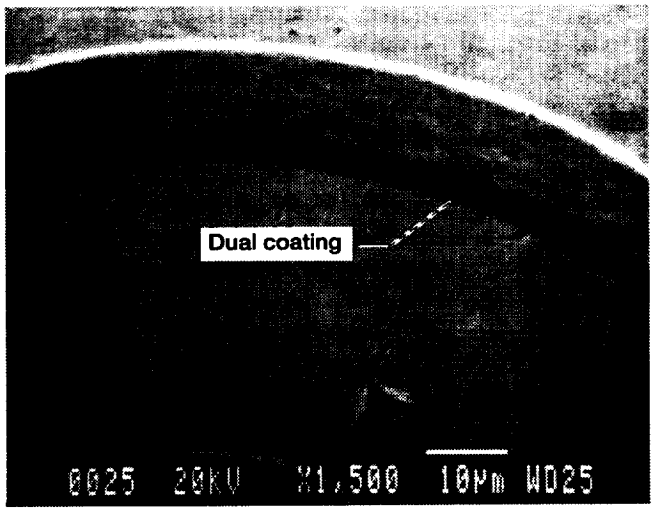

Figure 11.—SEM micrographs showing in-place and pushed out fibers in CVD SiC_f (SCS-6)/SAS composites.

REPORT DOCUMENTATION PAGE

Form Approved
OMB No. 0704-0188

1. AGENCY USE ONLY (*Leave blank*)	2. REPORT DATE	3. REPORT TYPE AND DATES COVERED
	July 1996	Technical Memorandum

4. TITLE AND SUBTITLE

Effects of Fiber Content on Mechanical Properties of CVD SiC Fiber Reinforced Strontium Aluminosilicate Glass-Ceramic Composites

5. FUNDING NUMBERS

WU-505-63-12

6. AUTHOR(S)

Narottam P. Bansal

7. PERFORMING ORGANIZATION NAME(S) AND ADDRESS(ES)

National Aeronautics and Space Administration
Lewis Research Center
Cleveland, Ohio 44135-3191

8. PERFORMING ORGANIZATION REPORT NUMBER

E-10341

9. SPONSORING/MONITORING AGENCY NAME(S) AND ADDRESS(ES)

National Aeronautics and Space Administration
Washington, D.C. 20546-0001

10. SPONSORING/MONITORING AGENCY REPORT NUMBER

NASA TM-107273

11. SUPPLEMENTARY NOTES

Responsible person, Narottam P. Bansal, organization code 5130, (216) 433-3855.

12a. DISTRIBUTION/AVAILABILITY STATEMENT

Unclassified - Unlimited
Subject Category 24

This publication is available from the NASA Center for AeroSpace Information, (301) 621-0390.

12b. DISTRIBUTION CODE

13. ABSTRACT (*Maximum 200 words*)

Unidirectional CVD SiC_f(SCS-6) fiber-reinforced strontium aluminosilicate (SAS) glass-ceramic matrix composites containing various volume fractions, ~ 16 to 40 volume %, of fibers were fabricated by hot pressing at 1400 °C for 2 h under 27.6 MPa. Monoclinic celsian, $SrAl_2Si_2O_8$, was the only crystalline phase formed, with complete absence of the undesired hexacelsian phase, in the matrix. Room temperature mechanical properties were measured in 3-point flexure. The matrix microcracking stress and the ultimate strength increased with increase in fiber volume fraction, reached maximum values for V_f ~ 0.35, and degraded at higher fiber loadings. This degradation in mechanical properties is related to the change in failure mode, from tensile at lower V_f to interlaminar shear at higher fiber contents. The extent of fiber loading did not have noticeable effect on either fiber-matrix debonding stress, or frictional sliding stress at the interface. The applicability of micromechanical models in predicting the mechanical properties of the composites was also examined. The currently available theoretical models do not appear to be useful in predicting the values of the first matrix cracking stress, and the ultimate strength of the SCS-6/SAS composites.

14. SUBJECT TERMS

Composites; Celsian; Glass-ceramic; Strength; Interfaces; Micromechanical models

15. NUMBER OF PAGES

27

16. PRICE CODE

A03

17. SECURITY CLASSIFICATION OF REPORT	18. SECURITY CLASSIFICATION OF THIS PAGE	19. SECURITY CLASSIFICATION OF ABSTRACT	20. LIMITATION OF ABSTRACT
Unclassified	Unclassified	Unclassified	

National Aeronautics and
Space Administration

Lewis Research Center
21000 Brookpark Rd.
Cleveland, OH 44135-3191